nanomaterials

MDPI

Article

Ultra-Thin SnS_2-Pt Nanocatalyst for Efficient Hydrogen Evolution Reaction

Yanying Yu †, Jie Xu †, Jianwei Zhang, Fan Li, Jiantao Fu, Chao Li * and Cuihua An *

Center for Electron Microscopy, TUT-FEI Joint Laboratory, Tianjin Key Laboratory of Advanced Porous Functional Materials, Institute for New Energy Materials & Low-Carbon Technologies, School of Materials Science and Engineering, Tianjin University of Technology, Tianjin 300384, China; yuyanying_link@163.com (Y.Y.); xujielink@163.com (J.X.); zhangjianwei248@163.com (J.Z.); lifan_96@163.com (F.L.); fujt2020@163.com (J.F.)

* Correspondence: chao_li@tjut.edu.cn (C.L.); ancuihua@tjut.edu.cn (C.A.); Tel.: +86-022-60215388 (C.L.); +86-022-60215388 (C.A.)

† These authors contributed equally to this work.

Received: 26 October 2020; Accepted: 20 November 2020; Published: 25 November 2020

Abstract: Transition-metal dichalcogenides (TMDs) materials have attracted much attention for hydrogen evolution reaction (HER) as a new catalyst, but they still have challenges in poor stability and high reaction over-potential. In this study, ultra-thin SnS_2 nanocatalysts were synthesized by simple hydrothermal method, and low load of Pt was added to form stable SnS_2-Pt-3 (the content of platinum is 0.5 wt %). The synergistic effect between ultra-thin SnS_2 rich in active sites and individual dispersed Pt nanoclusters can significantly reduce the reaction barrier and further accelerate HER reaction kinetics. Hence, SnS_2-Pt-3 exhibits a low overpotential of 210 mV at the current density of 10 mA cm^{-2}. It is worth noting that SnS_2-Pt-3 has a small Tafel slope (126 mV dec^{-1}) in 0.5 M H_2SO_4, as well as stability. This work provides a new option for the application of TMDs materials in efficient hydrogen evolution reaction. Moreover, this method can be easily extended to other catalysts with desired two-dimensional materials.

Keywords: ultra-thin SnS_2 nanocatalyst; Pt nanoclusters; synergistic effect; hydrogen evolution reaction

1. Introduction

Hydrogen is a considerable chemical commodity for its application in ammonia synthesis and petroleum refining [1–4]. Electrocatalysts for hydrogen evolution from water have been extensively studied for their advantages, having high purity and use in environmentally friendly products [5,6]. Now, Pt [7] and Pt-based catalysts have been considered as the most effective HER electrocatalysts reported in the literature [8]. However, the poor electrochemical stability, high production costs [9] and the raw material scarcity limits their mass production to meet the industrial demand. Therefore, the design HER catalyst of economic efficiency has become the key factor of electrocatalytic water splitting.

In recent years, the electrocatalytic properties of transition metal sulfides [10,11], carbides [12–14], borides [15], phosphides [16–18], nitrides [19–21] and oxides [22–24] have been increasingly studied, and electrocatalysts with low over-potential, high activity and high stability have been explored. Ultra-thin two-dimensional (2D) nanomaterials have unique bonding interaction methods, including single or few layers of transition metal carbon disulfide (TMD), metal oxides, etc. Strong covalent bonds extend through atoms in the plane, while weak van der Waals interactions exist between the layers. Weak interlayer bonding can easily peel these materials into thinner nanosheets containing several or single layers. These TMD ultra nanosheets usually exhibit anisotropy and have a larger

surface-to-volume ratio, thereby providing high-density surface active sites [25], which is a benefit to the application of HER catalyst. So, TMD nanosheets are alternative materials [26–28] of platinum-based catalyst for HER. SnS_2 is a typical two-dimensional material, which has the above-mentioned advantages of two-dimensional materials working as HER catalyst. However, the higher over-potential and Tafel slope in catalytic hydrogen evolution limit its application of HER catalyst. In our work, by doping Pt on the main carrier of SnS_2 nanosheets, the SnS_2-Pt composite catalyst was prepared. The SnS_2-Pt composite catalyst shows a lower over-potential and Tafel slope, compared with SnS_2 nanosheets. Using the synergistic effect [29,30] between SnS_2 and platinum, the hydrogen evolution performance is effectively promoted in this work.

Herein, we designed an efficient synthesis route to prepare dispersed Pt nanoparticles anchored on ultra-thin SnS_2 frameworks (SnS_2–Pt). The benefit of using SnS_2 cooperated with small amount of Pt, to help reduce the used amount of this precious metal, while keep the performance of the catalyst. The as-synthesized individual Pt nanoparticles are clearly identified through the aberration-corrected scanning transmission electron microscopy (AC-STEM). Furthermore, the ultra-thin SnS_2 combined with Pt nanoparticles can obviously enhance the conductivity, abundant exposed active sites and efficient transfer of the HER-related electrons, which endows SnS_2-Pt-3 with excellent HER activities in acidic electrolyte. The over-potential of the as prepared SnS_2-Pt-3 nanocatalyst is 210 mV under the current density of 10 mA cm^{-2}, while the Tafel slope of SnS_2-Pt-3 was 126 mV dec^{-1} in the electrolyte of 0.5 M H_2SO_4, as well as stability. This study provides a new way to design advanced SnS_2 catalyst with high activity, and meets the urgent needs of sustainable hydrogen economy.

2. Experimental Section

2.1. Chemicals

Tin (IV) chloride pentahydrate ($SnCl_4{\cdot}5H_2O$, AR), Thioacetamide (C_2H_5NS), Isopropyl Alcohol (C_3H_8O, AR), Chloroplatinic acid hexahydrate ($H_2PtCl_6{\cdot}6H_2O$), Sulfuric acid (H_2SO_4, GR), ethanol absolute (CH_3CH_2OH, AR) were obtained from Beijing Chemical Factory, Membrane solution and Commercial 20 wt % Pt/C were provided by Shanghai Hesen Electric Co., Ltd., Shanghai, China. The chemical reagents, used in the experimental preparation, are all of analytical purity and can be used directly without further decontamination. Ultrapure water was used in this word.

2.2. Synthesis

In this work, 0.35 g of crystalline tin tetrachloride and 0.3 g of thioacetamide (molar ratio: 1:4) were weighed and placed in a beakers, followed by 40 mL of isopropyl alcohol, which was stirred continuously for 30 min to form a uniform and transparent solution. Then, the solution was transferred to a 50 mL Teflon lined stainless steel autoclave. After that, the autoclave was sealed and placed in an oven and reacted at 180 °C for 24 h. The reactor was cooled to room temperature and the sediments were collected. The sediments were rinsed with ethanol and deionized water for several times, and centrifuged at 60 °C for 12 h to obtain ultra-thin nanometer SnS_2 catalyst.

The SnS_2 powder prepared above and hexahydrate of chloroplatinic acid (1 mmol/L) were dissolved in anhydrous ethanol at a mass ratio of 50:1, stirred continuously for 3 h, centrifuged and rinsed with deionized water for several times, dried at 12 h at 60 °C and calcined in vacuum at Ar 200 °C for 2 h to obtain SnS_2-Pt.

2.3. Characterization

The X-ray diffraction (XRD) pattern of SnS_2 nanocatalyst were measured on XRD instrument (Rigaku, SmartLab 9 KW, Japan). The range of 2θ was set at 10–75° and the scanning rate was set at 10° min^{-1}. The morphology of the SnS_2 nanocatalyst were obtained on Verios 460 L, and the structural characterization of SnS_2 nanocatalyst were carried on a High-Resolution Transmission Electron Microscope (Talos F200X, FEI, Hillsboro, OR, USA) and a Transmission Electron Microscope

with A Probe Corrector (Titan G2 300, FEI, Hillsboro, OR, USA). The X-ray photoelectron spectroscopy (XPS) and binding energy were calibrated with reference to C1's main peak of 284.8 eV.

2.4. Electrochemical Measurements

Altl electrochemical measurements [31–34] were performed in a typical three-electrode system on a CHI 760E electrochemical workstation at room temperature using a carbon paper (HCP030N, 0.3 mm of thick), modified with the catalysts as working electrode, an Ag/AgCl (in 0.5 M H_2SO_4) electrode as reference electrode, a carbon rod as the counter electrode. To prepare the catalyst ink, the catalyst (6 mg) was dissolved in anhydrous ethanol (500 microliter) and the Nafion (500 microliter) mixture of 0.5 wt % by ultrasonic dispersion for 30 min. The catalyst (200 microliter) was dropped on the surface of carbon paper (1 cm × 1 cm, with a load of 1.2 mg cm^{-2}) and dried at room temperature. SnS_2, SnS_2-Pt (scanning rate:10 mV s^{-1}) were subjected to linear scanning voltammetry (LSV) under the condition of 0.5 M H_2SO_4 (before HER measurement, the electrolyte was purified with pure N_2 gas for 30 min to remove the dissolved oxygen). Cyclic voltammetry (CV) scanning rate was 100 mV s^{-1}. By plotting the logarithmic current density of overpotential, the Tafel curve is obtained. Electrochemical impedance spectroscopy (EIS) was measured using the CHI 760E (Beijing, China) electrochemical workstation with an AC voltage amplitude of 5 mV and a frequency range of 0.01 Hz to 100 KHz at 0.5 M H_2SO_4. All data is compensated by i*R*. Electrochemical bi-layer capacitance (C_{dl}) for a binary free process was evaluated five times using cyclic volt-ampere method at five different scanning rates (25, 30, 35, 40 and 45 mV s^{-1}).

3. Results and Discussion

In this work, we synthesized ultra-thin SnS_2 nanosheets by a simple hydrothermal method [35,36] (see the Experimental Section for details), and further low-concentration Pt precursor to stir and adsorb to form SnS_2-Pt-3 materials, which were calcined to make the platinum particles and SnS_2 combine perfectly. By testing the hydrogen evolution performance of these four catalysts, we found that the SnS_2-Pt-3 catalyst has the best HER performance, so we focused on its structural characterization. The scanning electron microscopy (SEM) and transmission electron microscope (TEM) images are all shown phase and structure information of SnS_2-Pt-3 catalyst, while the results XPS are used to obtain the element valence state and composition analysis of SnS_2-Pt-3 catalyst. As shown in Figure 1, SnS_2-Pt-3 nanosheets were prepared according to the mass ratio of SnS_2 to $H_2PtCl_6{\cdot}H_2O$ (100 wt %: 5 wt %), in order to explore the influence of different Pt doping amount on catalytic hydrogen evolution performance, for comparison, we have prepared four different Pt-doping amount samples in our work. The amount of Pt are 0.04 wt %, 0.09 wt %, 0.5 wt % and 0.8 wt %, respectively. The four samples are renamed as SnS_2-Pt-1, SnS_2-Pt-2, SnS_2-Pt-3 and SnS_2-Pt-4, respectively.

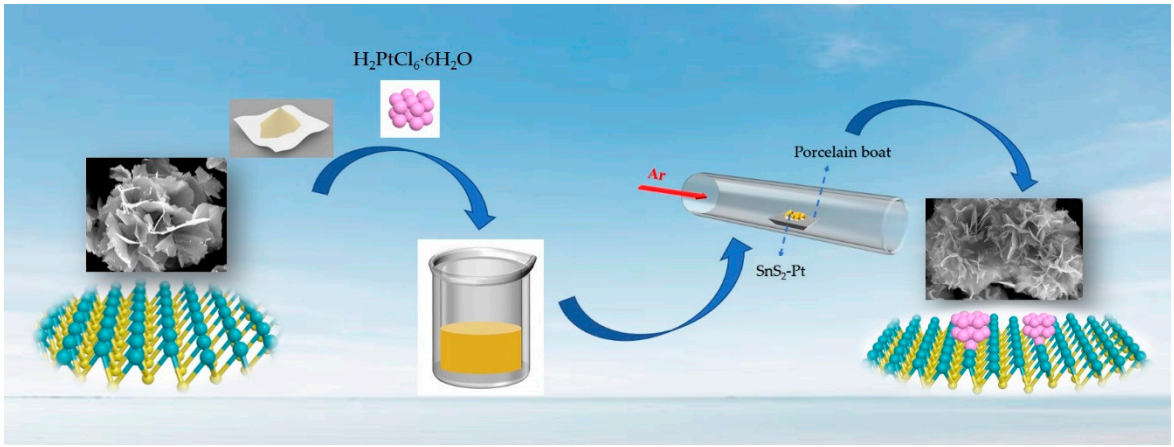

Figure 1. Synthesis diagram of ultra-thin SnS_2-Pt-3 nanosheets.

Figure 2a shows the SEM image, which is a flower-like SnS_2 nanostructure with similar morphology to pure SnS_2 (Figure S1a). By observing the low-magnification SEM image, no obvious large Pt clusters were found in SnS_2-Pt-3. The TEM image of SnS_2-Pt-3 is shown in Figure 2b. It can be seen that it is a very thin nanosheet, which is also confirmed in SEM image. By observing the high-resolution TEM (HRTEM) image (Figure 2c), we can see that the interfacial spacing d = 0.311 nm on surface (100) is very similar to the pure SnS_2 HRTEM image (Figure S1b). Figure 2d,e is atomic resolution high-angle annular dark-field scanning TEM (HAADF-STEM) images [37], which show some Pt clusters represented by red circles. By comparing the selected area electron diffraction (SAED) diagrams before, and after, doping, there is no obvious change in the interplanar spacing of SnS_2 (SnS_2 (100) plane with lattice spacing of 0.311 nm) (Figure 2c and Figure S1b). Inductively coupled plasma-atomic emission spectroscopy (ICP-MS) revealed that the Pt content of SnS_2-Pt-3 is 0.5 wt %. In addition, the HAADF image and the corresponding energy-dispersive X-ray spectroscopy (EDS) (Figure 2f) show that Sn, S and Pt element are uniformly distributed in SnS_2-Pt-3 nanosheets, and the corresponding element ratios are shown in Table S1.

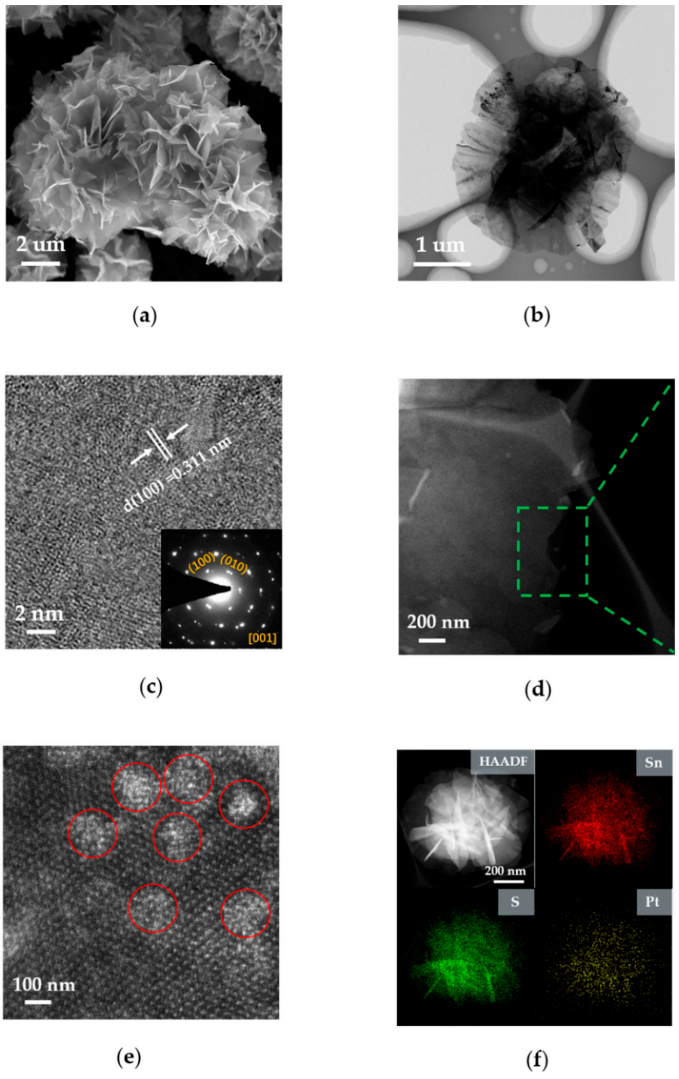

Figure 2. Structures of SnS_2-Pt-3. (**a**) The SEM image of SnS_2 nanostructure. (**b**) The TEM image of low-magnification morphology of SnS_2-Pt-3 nanosheets. (**c**) SnS_2-Pt-3 of high-resolution transmission diagram, in which is the corresponding SAED pattern. (**d**,**e**) Atomic resolution HAADF-STEM image with some individual Pt clusters represented by red circles. (**f**) The HAADF image and EDS mapping of Sn, S and Pt element from a SnS_2-Pt-3 nanosheet.

The X-ray photoelectron spectroscopy (XPS) was used to determine the elemental composition of SnS_2 nanosheets doped with different proportions of Pt precursor. As shown in the high-resolution XPS spectra of pure SnS_2 in Figure S2a,b, the two main peaks of Sn are $3d_{5/2}$ of 486.9 eV and $3d_{3/2}$ of 495.3 eV are in line with Sn^{4+}, and the two main peaks of S are $2p_{3/2}$ of 162.0 eV and $2p_{1/2}$ of 163.2 eV are assigned to S^{2-}, respectively [38]. By analyzing the distribution of Sn, S elements and the ratio of Sn/S (1:2) in the EDS mapping (Table S2) and the XRD diagram (Figure S2f), indicating that suggesting a rational stoichiometric composition of SnS_2. Besides, in the high-resolution XPS spectra of SnS_2-Pt-3 (Figure 3a,b), the Sn are $3d_{5/2}$ of 486.6 eV and $3d_{3/2}$ of 495.0 eV, and S are $2p_{3/2}$ of 161.7 eV and $2p_{1/2}$ of 162.9 eV and in the high-resolution XPS spectra of SnS_2-Pt-4 (Figure S2c–e), the Sn are $3d_{5/2}$ of 486.7 eV and $3d_{3/2}$ of 495.1 eV, and S are $2p_{3/2}$ of 161.8 eV and $2p_{1/2}$ of 163.0 eV. Compared with pure SnS_2, all the peak positions of Sn 3d and the S 2p regions in SnS_2-Pt-3 were lower binding energy shifted. Moreover, two Pt 4f peaks at 75.66 eV ($4f_{5/2}$) and 72.43 eV ($4f_{7/2}$) of SnS_2-Pt-3 (Figure 3c) and two Pt 4f peaks at 75.36 eV ($4f_{5/2}$) and 71.98 eV ($4f_{7/2}$) of SnS_2-Pt-4 (Figure S2e) were observed in the XPS spectrum, indicative of Pt^0. The detectable Pt^0 signal indicates that Pt crystal grains exist in SnS_2-Pt-3 and SnS_2-Pt-4, which further confirming HAADF-STEM and XRD results (Figure 2e and Figure S2f). The whole XPS spectrum of pure SnS_2, SnS_2-Pt-3 and SnS_2-Pt-4 is shown in Figure S3a. These three samples show similar chemical composition of Sn, S, Pt, O. No obvious change can be observed.

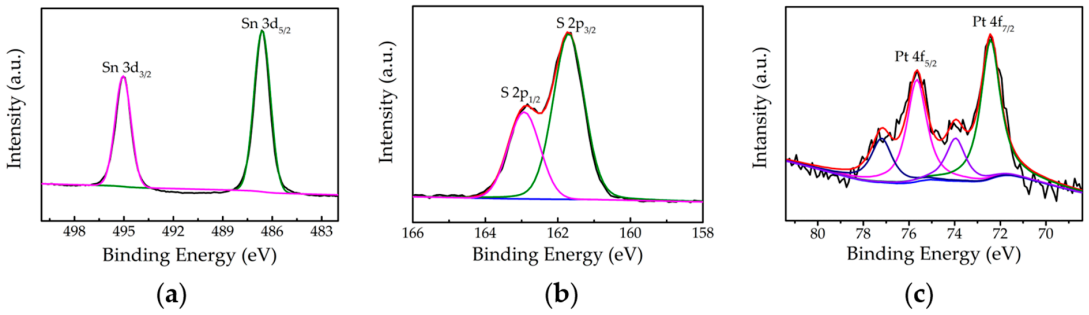

Figure 3. Chemical state analysis of SnS_2-Pt-3. (**a**,**b**) are Sn 3d and S 2p high-resolution XPS spectra of SnS_2-Pt-3. (**c**) the high-resolution XPS spectra of Pt 4f.

The HER performance of SnS_2-Pt-3 was measured by the carbon paper electrode test and compared against pure SnS_2, SnS_2-Pt-4 and commercial 20 wt % Pt/C in 0.5 M H_2SO_4 solution using a three-electrode system (see the Experimental Section for details) [39]. In order to reduce the experimental error caused by solution resistance, the initial data, obtained during the whole test process, were calibrated by ohmic potential drop unless special instructions, and all potential data obtained in this working electrochemical test were relative to reversible hydrogen electrode (RHE). The work electrode was scanned by CV several times until it reached a stable state. Figure 4a shows the LSV curve of the electrocatalytic hydrogen evolution of commercial Pt/C, pure SnS_2, SnS_2-Pt-3 and SnS_2-Pt-4 at a scanning speed of 10 mV s^{-1}. The cathode current of 10 mA cm^{-2} of SnS_2-Pt-3, only a low overpotential of 210 mV is needed, which is lower than pure SnS_2 (780 mV) and SnS_2-Pt-4 (250 mV) and not as good as commercial Pt/C (25 mV). It also proves that commercial Pt/C is indeed one of the best HER catalysts.

The Tafel slopes of SnS_2-Pt-3 and reference materials were linearly fitted (Figure 4b), and SnS_2 Pt-3 Tafel slopes was measured to be 126 mV dec^{-1}, which was smaller than that of pure SnS_2 (282 mV dec^{-1}) and SnS_2-Pt-4 (153 mV dec^{-1}), also indicating that the favorable electrocatalytic kinetics of SnS_2-Pt-3. According to related reports [40,41], the clustered catalyst can fully contact the surface active sites of the SnS_2 sample, thereby, optimizing the adsorption and release of hydrogen and promoting the role of catalytic hydrogen release. The catalyst in the form of platinum particles cannot fully contact the active sites due to its large size, which reduces the hydrogen evolution efficiency. By analyzing the TEM (HAADF-STEM) image (Figure S4), more Pt in SnS_2 (SnS_2-Pt-4) forms the particles in the sample, while Pt in SnS_2-Pt-3 forms the clusters, which makes SnS_2-Pt-3

nanosheets show excellent electrocatalytic performance in HER. The result further confirms that SnS_2-Pt-3 is an excellent electrocatalyst for HER. In order to verify, the electrochemical active surface area (ECSA) of the SnS_2-Pt-3 and reference materials were also evaluated by measuring electrochemical double-layer capacitance (C_{dl}). Select the non-Faraday region and measure the CV curves of Pt-C, pure SnS_2, SnS_2- Pt-1, SnS_2-Pt-2, SnS_2-Pt-3 and SnS_2-Pt-4 at scan rates of 25, 30, 35, 40 and 45 mV s^{-1} (Figure S5). The electrochemically active surface area of the catalyst was obtained by linear fitting. As shown in Figure 4c, the C_{dl} values of Pt-C, pure SnS_2, SnS_2-Pt-3 and SnS_2-Pt-4 catalysts are 5.9, 1.4, 6.3, and 4.4 mF cm^{-2}, respectively. The C_{dl} value of the SnS_2-Pt-3 catalyst is higher than that of Pt-C, because the doped platinum forms platinum clusters, which can improve the conductivity of the two-dimensional SnS_2 nanosheets, and promote faster interface charge transfer and clever electrochemistry catalysis. This confirms again that the hydrogen release efficiency of clustered platinum is better than that of platinum particles. In addition, electrochemical impedance spectroscopy (EIS) was conducted to study the influence of Pt clusters on the catalytic kinetics of electrocatalysts. As shown in Figure 4d, the charge transfer resistance (Rct) of SnS_2-Pt-3 is much smaller than that of pure SnS_2, indicating that the faster electron transfer and HER catalytic kinetics of SnS_2-Pt-3. In order to evaluate the stability of SnS_2-Pt-3 catalyst, continuous constant potential electrolysis is necessary for practical application. As shown in Figure 4e,f, the current density of SnS_2-Pt-3 did not decrease significantly over 20 h, and the electro-catalytic stability of SnS_2 Pt-3 could also be demonstrated after 1000 potential cycles.

By comparison with other synthesis methods (Table 1), we found that the SnS_2 prepared by hydrothermal method is not only simple in operation, but also has enough samples in one time. The SEM and TEM images show ultra-thin morphology and structure, which are not possessed by other preparation methods. SnS_2-Pt nanosheets were prepared by simple doping method, which greatly improved the electrocatalytic hydrogen evolution performance of SnS_2. Compared with other methods, the electrocatalytic hydrogen evolution performance of SnS_2 was significantly improved, which concludes that our research work is feasible and novel.

Table 1. Comparison table of electrocatalytic performance data of SnS_2 and its hybrids.

Electrode Material	Synthesis Method	Electrolyte	Overpotential at 10 mA/cm^2	Tafel Slope	Reference
SnS_2 SnS_2-Pt-3	Hydrothermal synthesis	0.5M H_2SO_4	−780 mV −210 mV	282 mV dec^{-1} 126 mV dec^{-1}	This work
SnS_2 MoS_2/SnS_2	Hydrothermal method	0.5 M H_2SO_4	−288 mV −580 mV	76 mV dec^{-1} 50 mV dec^{-1}	Ref [42]
$MoSe_2$ $MoSe_2/SnS_2$-2.5	Hydrothermal method	1.0 M KOH	−367 mV −285 mV	149 mV dec^{-1} 109 mV dec^{-1}	Ref [43]
MoS_2 MoS_2/SnS_2-2.5	Hydrothermal method	0.5 M H_2SO_4	−419 mV −343 mV	216 mV dec^{-1} 157 mV dec^{-1}	Ref [43]
SnS_2 SnS_2/G	Solid-state ball-milling approach	1.0 M KOH	−600 mV −360 mV	375 mV dec^{-1} 257 mV dec^{-1}	Ref [44]
SnS_2 $Sn_{0.3}W_{0.7}S_2$	Hydrothermal method	0.5 M H_2SO_4	−481 mV −345 mV	398 mV dec^{-1} 114 mV dec^{-1}	Ref [45]
SnS_2 5% Mo-SnS 10% Mo-SnS	Colloidal technique	0.5 M H_2SO_4	−600 mV −486 mV −377 mV	328 mV dec^{-1} 177 mV dec^{-1} 100 mV dec^{-1}	Ref [46]

In additions, we also performed SnS_2-Pt-1 and SnS_2-Pt-2 HER performance (Figure 5a), and the results showed that the over-potential at 10 mA cm^{-2} current density was 290 mV and 320 mV, respectively, which were higher than SnS_2-Pt-3. The measured Tafel slopes of SnS_2-Pt-1 and SnS_2-Pt-2

(Figure 5b) are 176 mV dec^{-1}, and 184 mV dec^{-1}, respectively. These results indicating a faster hydrogen insertion/extraction kinetics for SnS_2-Pt-3. Meanwhile, the C_{dl} value of SnS_2-Pt-1 and SnS_2-Pt-2 are 3.8 mF cm^{-2} and 3.4 mF cm^{-2} (Figure 5c), also further indicating the improved electrochemically active sites of SnS_2-Pt-3. Figure 5d shows the XRD patterns of SnS_2-Pt-1 and SnS_2-Pt-1, which indicates that the phase and structure information of them has no significant change compared to pure SnS_2.

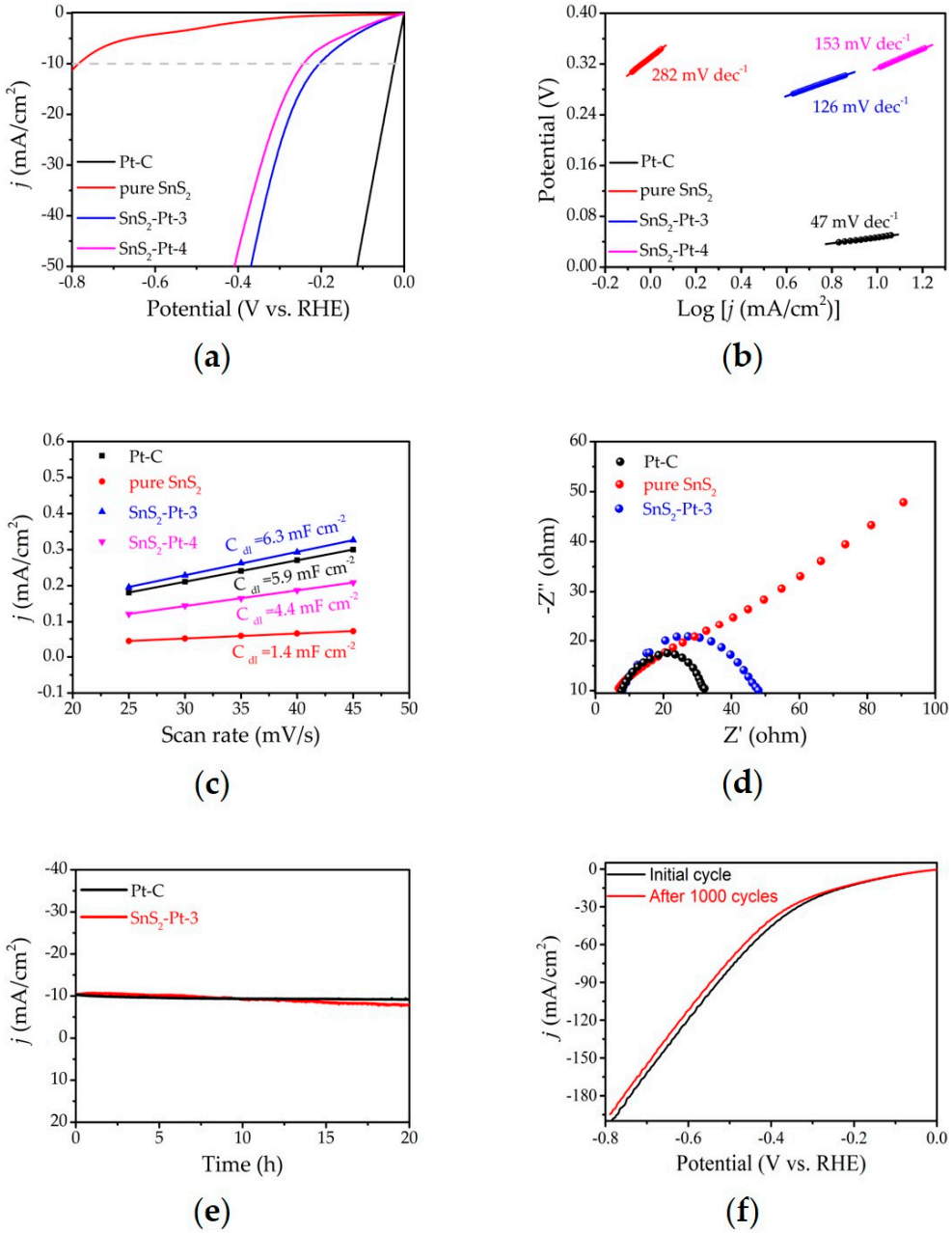

Figure 4. HER of the SnS_2-Pt-3. (**a**) LSV curves of the commercial Pt/C, the pure SnS_2 nanosheets and the SnS_2-Pt-3 ones. (**b**) Tafel plots corresponding to (**a**). (**c**) Electrochemical active surface area with different mass ratio. (**d**) EIS measurement of pure SnS_2 and SnS_2-Pt-3. (**e**) I-T distribution diagram of SnS_2-Pt-3 nanosheets. (**f**) LSV curves of the SnS_2-Pt-3 before and after 1000 potential cycles.

In addition, after a long-term catalytic process, the HAADF-STEM images (Figure S6a,b), XRD (Figure S6f) showed no significant changes, indicating that the morphology and structure of HAADF-STEM were well preserved. The XPS of SnS_2-Pt-3 samples that have been tested for 20 h, the Sn are $3d_{5/2}$ of 487.06 eV and $3d_{3/2}$ of 495.49 eV, and S are $2p_{3/2}$ of 162.18 eV and $2p_{1/2}$ of 163.37 eV,

two Pt 4f peaks at 76.12 eV ($4f_{5/2}$) and 72.85 eV ($4f_{7/2}$). The whole XPS spectrum is shown in Figure S3b, no obvious change can be observed, which further confirmed its excellent structural stability.

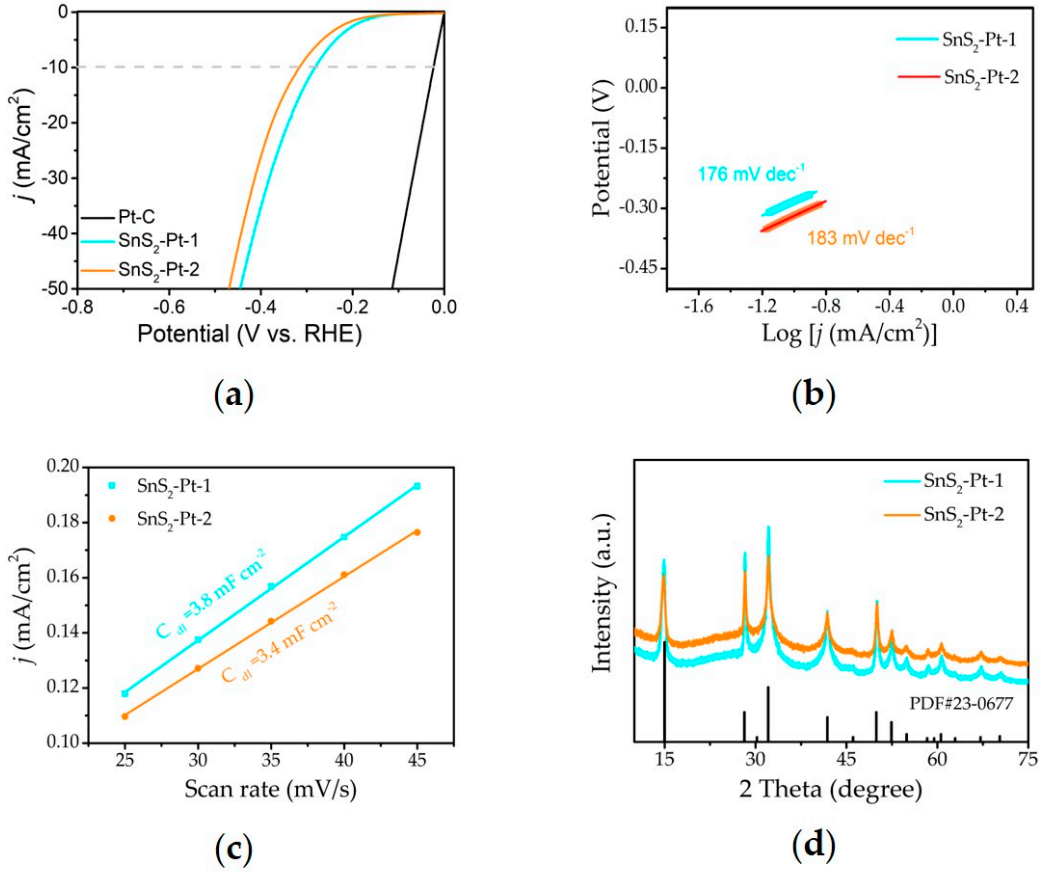

Figure 5. Structural and performance characterization of SnS_2-Pt-1 and SnS_2-Pt-2. (**a**) The LSV curves under hydrogen evolution. (**b**) The Tafel slopes. (**c**) Electrochemical active surface area. (**d**) XRD.

4. Conclusions

In summary, ultra-thin SnS_2 nanosheets were prepared by a simple hydrothermal synthesis method, and then small Pt clusters were anchored on ultra-thin SnS_2 to form SnS_2-Pt-3 nanosheets. Furthermore, compared with pure ultra-thin SnS_2, the prepared ultra-thin SnS_2-Pt-3 nanosheets shows obviously superior HER performance. Under the current density of 10 mA cm^{-2}, its overpotential was 210 mV and its Tafel slope was 126 mV dec^{-1} in 0.5 M H_2SO_4 and no obvious attenuation phenomenon was observed after 20 h chronoamperometry, as well as stability. All these indicate that SnS_2-Pt-3 nanosheets catalyst have broad application prospects in H_2 production, energy supply and electrochemical reaction. This prominent HER performance is due to the collaborative effect between the ultra-thin nanosheet structure and Pt clusters, which together enhance the active site of the catalyst. Our work also proves that synergy is an available strategy to improve the electrocatalytic performance of two-dimensional materials.

Supplementary Materials: The following are available online at http://www.mdpi.com/2079-4991/10/12/2337/s1, Figure S1: Nanosheet structure of pure SnS_2, Table S1: SnS_2-Pt-3 nanosheet EDS and corresponding element ratio, Figure S2: Chemical structure analysis of pure SnS_2 and SnS_2-Pt-4, Table S2. Pure SnS_2 nanosheet EDS and corresponding element ratio, Figure S3. The whole XPS spectrum, Figure S4. (a) SEM and (b) TEM of SnS_2-Pt-4, Figure S5. Double-layer capacitance measurements, Figure S6. Structure and performance characterization diagram of SnS_2-Pt-3 after 20-h test.

Author Contributions: C.L., and C.A. designed the research project and supervised the experiments. Y.Y. synthesized SnS_2 and SnS_2-Pt nanocatalysts, J.X. carried out TEM experiments and analyzed data with the

help of C.L., C.A., J.Z., F.L. and J.F., Y.Y., J.X. and C.L. wrote the paper, in which the results and text are discussed by all the authors. All authors have read and agreed to the published version of the manuscript.

Funding: The National Natural Science Foundation of China (No. 11604241, 51601127, 61705115), the Young Elite Scientists Sponsorship Program by Tianjin, the Tianjin Municipal Science and Technology Commission (19JCQNJC15100, 18JCYBJ90200). The APC was funded by the Young Elite Scientists Sponsorship Program by Tianjin.

Acknowledgments: This work was supported by the National Natural Science Foundation of China (No. 11604241, 51601127, 61705115), the Young Elite Scientists Sponsorship Program by Tianjin, the Tianjin Municipal Science and Technology Commission (19JCQNJC15100, 18JCYBJ90200).

Conflicts of Interest: The authors declare no conflict of interest.

References

1. Dresselhaus, M.S.; Thomas, I.L. Alternative energy technologies. *Nature* **2001**, *414*, 332–337. [CrossRef] [PubMed]
2. Tan, Y.; Wang, H.; Liu, P.; Cheng, C.; Zhu, F.; Hirata, A.; Chen, M. 3D Nanoporous metal phosphides toward high-efficiency electrochemical hydrogen production. *Adv. Mater.* **2016**, *28*, 2951–2955. [CrossRef] [PubMed]
3. Deng, J.; Ren, P.; Deng, D.; Yu, L.; Yang, F.; Bao, X. Highly active and durable non-precious-metal catalysts encapsulated in carbon nanotubes for hydrogen evolution reaction. *Energy Environ. Sci.* **2014**, *7*, 1919–1923. [CrossRef]
4. Kibsgaard, J.; Tsai, C.; Chan, K.; Benck, J.D.; Nørskov, J.K.; Abild-Pedersen, F.; Jaramillo, T.F. Designing an improved transition metal phosphide catalyst for hydrogen evolution using experimental and theoretical trends. *Energy Environ. Sci.* **2015**, *8*, 3022–3029. [CrossRef]
5. Staszak-Jirkovsky, J.; Malliakas, C.D.; Lopes, P.P.; Danilovic, N.; Kota, S.S.; Chang, K.C.; Genorio, B.; Strmcnik, D.; Stamenkovic, V.R.; Kanatzidis, M.G.; et al. Design of active and stable Co-Mo-S_x chalcogels as pH-universal catalysts for the hydrogen evolution reaction. *Nat. Mater.* **2016**, *15*, 197–203. [CrossRef] [PubMed]
6. Stamenkovic, V.R.; Strmcnik, D.; Lopes, P.P.; Markovic, N.M. Energy and fuels from electrochemical interfaces. *Nat. Mater.* **2017**, *16*, 57–69. [CrossRef]
7. Popczun, E.J.; Read, C.G.; Roske, C.W.; Lewis, N.S.; Schaak, R.E. Highly active electrocatalysis of the hydrogen evolution reaction by cobalt phosphide nanoparticles. *Angew. Chem. Int. Ed.* **2014**, *53*, 5427–5430. [CrossRef]
8. Ma, Z.; Tian, H.; Meng, G.; Peng, L.; Chen, Y.; Chen, C.; Chang, Z.; Cui, X.; Wang, L.; Jiang, W.; et al. Size effects of platinum particles@CNT on HER and ORR performance. *Sci. China Mater.* **2020**, in press. [CrossRef]
9. Zheng, Y.; Jiao, Y.; Jaroniec, M.; Qiao, S. Advancing the electrochemistry of the hydrogen-evolution reaction through combining experiment and theory. *Angew. Chem. Int. Ed.* **2015**, *54*, 52–65. [CrossRef]
10. Luo, J.; Im, J.H.; Mayer, M.T.; Schreier, M.; Nazeeruddin, M.K.; Park, N.G.; Tilley, S.D.; Fan, H.J.; Gratzel, M. Water photolysis at 12.3% efficiency via perovskite photovoltaics and Earth-abundant catalysts. *Science* **2014**, *345*, 1593–1596. [CrossRef]
11. Durst, J.; Siebel, A.; Simon, C.; Hasché, F.; Herranz, J.; Gasteiger, H.A. New insights into the electrochemical hydrogen oxidation and evolution reaction mechanism. *Energy Environ. Sci.* **2014**, *7*, 2255–2260. [CrossRef]
12. Balogun, M.S.; Qiu, W.; Yang, H.; Fan, W.; Huang, Y.; Fang, P.; Li, G.; Ji, H.; Tong, Y. A monolithic metal-free electrocatalyst for oxygen evolution reaction and overall water splitting. *Energy Environ. Sci.* **2016**, *9*, 3411–3416. [CrossRef]
13. Chen, Z.; Ye, S.; Wilson, A.R.; Ha, Y.-C.; Wiley, B.J. Optically transparent hydrogen evolution catalysts made from networks of copper–platinum core–shell nanowires. *Energy Environ. Sci.* **2014**, *7*, 1461–1467. [CrossRef]
14. Chen, J.; Yu, D.; Liao, W.; Zheng, M.; Xiao, L.; Zhu, H.; Zhang, M.; Du, M.; Yao, J. WO_{3-x} nanoplates grown on carbon nanofibers for an efficient electrocatalytic hydrogen evolution reaction. *ACS Appl. Mater. Interfaces* **2016**, *8*, 18132–18139. [CrossRef] [PubMed]
15. Xu, L.; Jiang, Q.; Xiao, Z.; Li, X.; Huo, J.; Wang, S.; Dai, L. Plasma-engraved Co_3O_4 nanosheets with oxygen vacancies and high surface area for the oxygen evolution reaction. *Angew. Chem. Int. Ed.* **2016**, *55*, 5277–5281. [CrossRef]
16. Lu, X.F.; Gu, L.F.; Wang, J.W.; Wu, J.X.; Liao, P.Q.; Li, G.R. Bimetal-organic framework derived $CoFe_2O_4$/C porous hybrid nanorod arrays as high-performance electrocatalysts for oxygen evolution reaction. *Adv. Mater.* **2017**, *29*, 1604437. [CrossRef]

17. Lai, F.; Miao, Y.E.; Huang, Y.; Zhang, Y.; Liu, T. Nitrogen-doped carbon nanofiber/molybdenum disulfide nanocomposites derived from bacterial cellulose for high-efficiency electrocatalytic hydrogen evolution reaction. *ACS Appl. Mater. Interfaces* **2016**, *8*, 3558–3566. [CrossRef]
18. Yang, Y.; Fei, H.; Ruan, G.; Li, Y.; Tour, J.M. Vertically aligned WS_2 nanosheets for water splitting. *Adv. Funct. Mater.* **2015**, *25*, 6199–6204. [CrossRef]
19. Youn, D.H.; Han, S.; Kim, J.Y.; Kim, J.Y.; Park, H.; Choi, S.H.; Lee, J.S. Highly active and stable hydrogen evolution electrocatalysts based on molybdenum compounds on carbon nanotube-graphene hybrid support. *ACS Nano* **2014**, *8*, 5164–5173. [CrossRef]
20. Yu, Y.; Huang, S.; Li, Y.; Steinmann, S.N.; Yang, W.; Cao, L. Layer-dependent electrocatalysis of MoS_2 for hydrogen evolution. *Nano Lett.* **2014**, *14*, 553–558. [CrossRef]
21. Xie, J.; Li, S.; Zhang, X.; Zhang, J.; Wang, R.; Zhang, H.; Pan, B.; Xie, Y. Atomically-thin molybdenum nitride nanosheets with exposed active surface sites for efficient hydrogen evolution. *Chem. Sci.* **2014**, *5*, 4615–4620. [CrossRef]
22. Wan, C.; Regmi, Y.N.; Leonard, B.M. Multiple phases of molybdenum carbide as electrocatalysts for the hydrogen evolution reaction. *Angew. Chem. Int. Ed.* **2014**, *53*, 6407–6410. [CrossRef] [PubMed]
23. Fan, M.; Chen, H.; Wu, Y.; Feng, L.; Liu, Y.; Li, G.; Zou, X. Growth of molybdenum carbide micro-islands on carbon cloth toward binder-free cathodes for efficient hydrogen evolution reaction. *J. Mater. Chem. A* **2015**, *3*, 16320–16326. [CrossRef]
24. Vrubel, H.; Hu, X. Molybdenum boride and carbide catalyze hydrogen evolution in both acidic and basic solutions. *Angew. Chem. Int. Ed.* **2012**, *51*, 12703–12706. [CrossRef]
25. Chia, X.; Pumera, M. Characteristics and performance of two-dimensional materials for electrocatalysis. *Nat. Catal.* **2018**, *1*, 909–921. [CrossRef]
26. Xue, Z.; Su, H.; Yu, Q.; Zhang, B.; Wang, H.; Li, X.; Chen, J. Janus Co/CoP nanoparticles as efficient mott-schottky electrocatalysts for overall water splitting in wide pH range. *Adv. Eng. Mater.* **2017**, *7*, 1602355. [CrossRef]
27. Wang, H.; Xiao, X.; Liu, S.; Chiang, C.L.; Kuai, X.; Peng, C.K.; Lin, Y.C.; Meng, X.; Zhao, J.; Choi, J.; et al. Structural and electronic optimization of MoS_2 edges for hydrogen evolution. *J. Am. Chem. Soc.* **2019**, *141*, 18578–18584. [CrossRef]
28. Wu, L.; Longo, A.; Dzade, N.Y.; Sharma, A.; Hendrix, M.; Bol, A.A.; de Leeuw, N.H.; Hensen, E.J.M.; Hofmann, J.P. The origin of high activity of amorphous MoS_2 in the hydrogen evolution reaction. *Chem. Sustain. Chem.* **2019**, *12*, 4383–4389. [CrossRef]
29. Wang, Y.; Sun, W.; Ling, X.; Shi, X.; Li, L.; Deng, Y.; An, C.; Han, X. Controlled synthesis of Ni-doped MoS_2 hybrid electrode for synergistically enhanced water-splitting process. *Chemistry* **2019**, in press. [CrossRef]
30. Xiao, W.; Liu, P.; Zhang, J.; Song, W.; Feng, Y.; Gao, D.; Ding, J. Dual-functional N dopants in edges and basal plane of MoS_2 nanosheets toward efficient and durable hydrogen evolution. *Adv. Energy Mater.* **2017**, *7*, 1602086. [CrossRef]
31. Nikand, B.; Khalilzadeh, M.A. Liquid phase determination of bisphenol A in food samples using novel nanostructure ionic liquid modified sensor. *J. Mol. Liq.* **2016**, *215*, 253–257.
32. Khalilzadeh, M.A.; Karimi-Maleh, H.; Gupta, V.K. A nanostructure based electrochemical sensor for square wave voltammetric determination of L-Cysteine in the presence of high concentration of folic acid. *Electroanalysis* **2015**, *27*, 1766–1773. [CrossRef]
33. Khalilzadeh, M.A.; Arab, Z. High Sensitive Nanostructure Square Wave Voltammetric sensor for determination of vanillin in food samples. *Curr. Anal. Chem.* **2017**, *13*, 81–86. [CrossRef]
34. Ashjari, M.; Karimi-Maleh, H.; Ahmadpour, F.; Shabani-Nooshabadi, M.; Sadrnia, A.; Khalilzadeh, M.A. Voltammetric analysis of mycophenolate mofetil in pharmaceutical samples via electrochemical nanostructure based sensor modified with ionic liquid and MgO/SWCNTs. *J. Taiwan Inst. Chem. E* **2017**, *80*, 989–996. [CrossRef]
35. Mali, J.M.; Arbuj, S.S.; Ambekar, J.D.; Rane, S.B.; Mulik, U.P.; Amalnerkar, D.P. Hydrothermal synthesis of SnS_2 faceted nano sheets and their visible light driven photocatalytic performance. *Sci. Adv. Mater.* **2013**, *5*, 1994–1998. [CrossRef]
36. Tian, H.; Fan, C.; Liu, G.; Zhang, Y.; Wang, M.; Li, E. Hydrothermal synthesis and fast photoresponsive characterization of SnS_2 hexagonal nanoflakes. *J. Mater. Sci.* **2019**, *54*, 2059–2065. [CrossRef]
37. Xu, J.; He, J.; Ding, Y.; Luo, J. X-ray imaging of atomic nuclei. *Sci. China Mater.* **2020**, *63*, 1788–1796. [CrossRef]

38. Xu, J.; Lai, S.; Hu, M.; Ge, S.; Xie, R.; Li, F.; Hua, D.; Xu, H.; Zhou, H.; Wu, R. Semimetal 1H-SnS_2 enables high-efficiency electroreduction of CO_2 to CO. *Small Methods* **2020**, *4*, 2000567. [CrossRef]
39. Xu, J.; Zhang, C.; Liu, H.; Sun, J.; Xie, R.; Qiu, Y.; Lü, F.; Liu, Y.; Zhuo, L.; Liu, X.; et al. Amorphous MoO_X-Stabilized single platinum atoms with ultrahigh mass activity for acidic hydrogen evolution. *Nano Energy* **2020**, *70*, 104529. [CrossRef]
40. Zhou, M.; Bao, S.; Bard, A.J. Probing Size and Substrate Effects on the Hydrogen Evolution Reaction by Single Isolated Pt Atoms, Atomic Clusters, and Nanoparticles. *J. Am. Chem. Soc.* **2019**, *141*, 7327–7332. [CrossRef]
41. Cheng, X.; Li, Y.; Zheng, L.; Yan, Y.; Zhang, Y.; Chen, G.; Sun, S.; Zhang, J. Highly active, stable oxidized platinum clusters as electrocatalysts for the hydrogen evolution reaction. *Energy Environ. Sci.* **2017**, *10*, 2450–2458. [CrossRef]
42. Xiao, X.; Wang, Y.; Xu, X.; Yang, T.; Zhang, D. Preparation of the flower-like MoS_2/SnS_2 heterojunction as an efficient electrocatalyst for hydrogen evolution reaction. *Mol. Catal.* **2020**, *487*, 110890. [CrossRef]
43. Chen, Y.; Wang, X.; Lao, M.; Rui, K.; Zheng, X.; Yu, H.; Ma, J.; Dou, S.; Sun, W. Electrocatalytically inactive SnS_2 promotes water adsorption/dissociation on molybdenum dichalcogenides for accelerated alkaline hydrogen evolution. *Nano Energy* **2019**, *64*, UNSP 103918. [CrossRef]
44. Lonkar, S.P.; Pillai, V.V.; Patole, S.P.; Alhassan, S.M. Scalable in situ synthesis of 2D-2D-Type graphene-wrapped SnS_2 nanohybrids for enhanced supercapacitor and electrocatalytic applications. *ACS Appl. Energy Mater.* **2020**, *3*, 4995–5005. [CrossRef]
45. Shao, G.; Xue, X.; Wu, B.; Lin, Y.; Ouzounian, M.; Hu, T.S.; Xu, Y.; Liu, X.; Li, S.; Suenaga, K.; et al. Template-assisted synthesis of metallic 1T ′-$Sn_{0.3}W_{0.7}S_2$ nanosheets for hydrogen evolution reaction. *Adv. Funct. Mater.* **2020**, *30*, 1906069. [CrossRef]
46. Kadam, S.R.; Ghosh, S.; Bar-Ziv, R.; Bar-Sadan, M. Structural transformation of SnS_2 to SnS by Mo doping produces electro/photocatalyst for hydrogen production. *Chem. Eur. J.* **2020**, *26*, 6679–6685. [CrossRef]